PCCP

PAPER

View Article Online
View Journal | View Issue

Cite this: *Phys. Chem. Chem. Phys.*, 2015, **17**, 11763

Phase stability, chemical bonding and mechanical properties of titanium nitrides: a first-principles study†

Shuyin Yu,*[ab] Qingfeng Zeng,[ab] Artem R. Oganov,[bcd] Gilles Frapper[e] and Litong Zhang[a]

Received 11th January 2015,
Accepted 26th March 2015

DOI: 10.1039/c5cp00156k

www.rsc.org/pccp

We have performed first-principles evolutionary searches for stable Ti–N compounds and have found, in addition to the well-known rock-salt TiN, new ground states Ti_3N_2, Ti_4N_3, Ti_6N_5 at atmospheric pressure, and Ti_2N and TiN_2 at higher pressures. The latter nitrogen-rich structure contains encapsulated N_2 dumbbells with a N–N distance of 1.348 Å at 60 GPa. TiN_2 is predicted to be mechanically stable and quenchable. Our calculations on the mechanical properties (bulk modulus, shear modulus, Young's modulus, Poisson's ratio, and hardness) are in excellent agreement with the available experimental data. Further analyses of the electronic density of states, crystal orbital Hamilton population and the electron localization function reveal that the hardness is enhanced by strengthening directional covalent bonds and disappearance of Ti–Ti metallic bonding.

1 Introduction

The discovery of new ultra-incompressible materials with novel mechanical and electronic properties is of great fundamental interest and practical importance.[1] Titanium nitride and its derivatives are materials which have many remarkable properties, such as chemical stability, thermal stability, oxidative resistance, good adhesion to the substrate, high fracture toughness and high hardness, which lend themselves to a wide range of applications. Their high hardness and corrosion resistance have made it particularly useful for increasing the wear resistance of high speed steel cutting tools,[2] while their high conductivity and diffusion barrier have led to their use in semiconductor metallization schemes.[3] In addition, titanium nitride and its derivatives also have been used for tool bit coatings, cosmetic faux gold surfaces, thin film resistors, wavelength selective transparent optical films,[4] and energy-saving coatings for windows due to their strong infrared reflection.

Numerous studies have been done not only on stoichiometric rock-salt TiN, but also on the under-stoichiometric TiN_x ($0.67 \leq x \leq 1$).[5] There are numerous reports on the phase stability, elasticity, electronic, chemical bonding properties[6–8] and film growth[9–11] *etc.*, from the early studies of Blaha and Schwarz in the 1980s[12,13] to the more recent studies.[14–16] However, most of their studies focus on the stoichiometric rock-salt TiN, and there are few studies of non-stoichiometric titanium nitrides. Many metals have numerous nitrides, and the question of how many titanium nitride phases do really exist is still a mystery. With this in mind, we decided to explore the crystal structures and possible stoichiometries in the Ti–N system by applying modern computational techniques of the recently developed evolutionary algorithm (USPEX).

TiN was first separated by Story–Maskelyne[17] from a meteorite, and it crystallizes into the well-known rock-salt structure. However, the pressure of phase transformation from rock-salt to CsCl-type structure is still controversial.[18–20] The other known compounds are Ti_2N and Ti_3N_4. ε-Ti_2N[21] ($P4_2/mnm$) is the most stable phase of Ti_2N under normal conditions, while the δ′ phase ($I4_1/amd$) can only exist at high temperatures.[22] Ivashchenko *et al.*[23] predicted phase transformation sequence ε-Ti_2N → Au_2Te-type → Al_2Cu-type with transition pressures of 77.5 and 86.7 GPa, respectively. For the metastable Ti_3N_4, Kroll *et al.*[24] proposed that it adopts the $CaTi_2O_4$-type structure under normal conditions. Upon increasing the pressure, it was proposed

[a] *Science and Technology on Thermostructural Composite Materials Laboratory, School of Materials Science and Engineering, Northwestern Polytechnical University, Xi'an, Shaanxi 710072, P. R. China. E-mail: yushuyin2014@gmail.com*
[b] *International Center for Materials Discovery, School of Materials Science and Engineering, Northwestern Polytechnical University, Xi'an, Shaanxi 710072, P. R. China*
[c] *Department of Geosciences, Center for Materials by Design, and Institute for Advanced Computational Science, State University of New York, Stony Brook, NY 11794-2100, USA*
[d] *Moscow Institute of Physics and Technology, Dolgoprudny, Moscow Region 141700, Russia*
[e] *IC2MP UMR 7285, Université de Poitiers, CNRS, 4, rue Michel Brunet, TSA 51106, 86073 Poitiers Cedex 9, France*

† Electronic supplementary information (ESI) available. See DOI: 10.1039/c5cp00156k

to transform first into the Zr_3N_4-type structure, and then into the cubic Th_3P_4-type structure.

Although titanium nitrides have been studied for decades, a detailed theoretical study of their phase equilibria, electronic and mechanical properties would help to reconcile controversies and possibly predict new technologically useful materials. This is exactly the purpose of the present paper. We hope this study will provide guidance for experimental groups aiming to synthesize those novel crystal structures.

2 Computational methodology

To find all potential Ti_xN_y structures in the binary Ti–N phase diagram, we performed an extensive computational search for stable compounds by using the evolutionary algorithm approach as implemented in the USPEX code[25–27] in its variable-composition mode,[28] interfaced using the VASP density-functional package.[29] Evolutionary predictions were performed at pressures 0, 20 and 60 GPa and the number of atoms was allowed up to 24 atoms in a primitive cell. The first generation of structures was produced randomly, and the subsequent generations were obtained by applying heredity (50%), atom transmutation (20%), and lattice mutation (15%) operators, while some were produced randomly (15%). These are typical parameters for USPEX calculations, with which the efficiency is known to be very high. The details of the search algorithm and its first several applications have been described elsewhere.[30]

The first-principles electronic structure calculations were carried out within the framework of density functional theory (DFT)[31,32] within the generalized gradient approximation (GGA) in the Perdew–Burke–Ernzerhof (PBE) form.[33] The interactions between the ions and the electrons are described by the projector-augmented wave (PAW) method[34] with a cutoff energy of 600 eV. The exchange–correlation functional based on the local density approximation (LDA)[35] was also considered in our present work for comparison. The Brillouin zone was sampled by uniform Γ-centered Monkhorst–Pack meshes[36] with the resolution of $2\pi \times 0.03$ Å^{-1}, which ensures that the error bars of total energies are less than 1 meV per atom. Besides, all forces on atoms were converged to less than 1 meV Å^{-1} and the total stress tensor was hydrostatic in the order of 0.01 GPa.

Here we have chosen not to use any special approaches for strongly correlated electrons. One approach, hybrid functionals, is applicable only to insulators – *i.e.* is not suitable for variable-composition systems and chemical reactions involving metals (*e.g.* metallic Ti). Another popular approach, DFT + U, requires parameter U, which depends on the valence state – which can be critical for variable-composition calculations involving multiple-valence atoms (such as titanium). At the same time, electron correlations are much less important for early 3d-metals (such as Sc, and Ti) than for late 3d-metals (such as Fe, Co, and Ni). Our choice of standard DFT is validated by the fact that our search at atmospheric pressure has found all known stable compounds and their crystal structures. With increasing pressure electron correlations decrease and DFT (LDA and GGA) becomes even more reliable.

Theoretical phonon spectra were calculated based on the supercell method using the PHONOPY package[37] in order to probe the dynamic stability of the predicted Ti_xN_y compounds at different pressures. The elastic constants were calculated from the stress–strain relationship, and Voigt–Reuss–Hill (VRH) approximation[38–40] was employed to obtain the bulk modulus B, shear modulus G, Young's modulus E, and Poisson's ratio ν. The theoretical Vickers hardness H_v was estimated by using the Chen's model[41] both at GGA and LDA levels, according to the expression:

$$H_v = 2(\kappa^2 G)^{0.585} - 3 \quad (1)$$

where κ is the Pugh ratio: $\kappa = G/B$. The directional dependence of the Young's modulus for crystals of different symmetries encountered in this study is given in the ESI.†

3 Results and discussion

Thermodynamics of titanium nitrides can be quantified by constructing the thermodynamic convex hull, which is a complete set of phases stable against transformation into any other phases and decomposition into any set of other phases. These thermodynamically stable phases can be synthesized in principle.[42] The convex hull curves were reconstructed after phonon calculations for the selected thermodynamically stable phases, which are shown in Fig. 1 and Fig. S6 (ESI†). Noticeably, our evolutionary simulations succeed in finding the well-known rock-salt TiN and ε-Ti_2N observed by experiments under ambient conditions. In addition, we uncovered three new stable compounds, the orthorhombic Ti_3N_2, and monoclinic Ti_4N_3 and Ti_6N_5. At 20 GPa, only the *Immm*-Ti_3N_2 phase loses its thermodynamic stability, *i.e.*, becomes a metastable phase. At a higher pressure of 60 GPa, ε-Ti_2N transforms into the orthorhombic *Cmcm* phase, and a new stable nitrogen-rich compound TiN_2 is discovered.

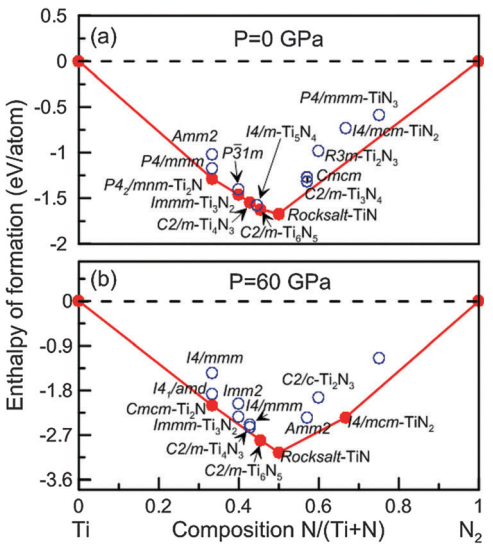

Fig. 1 Convex hull diagrams for the Ti–N system at 0 (a) and at 60 GPa (b). Circles denote stable (solid circles) and metastable (open circles) structures. The hexagonal ω-Ti[43] and α-N_2[44] are adopted as reference states.

The detailed crystallographic data and enthalpies of formation are listed in Table 1S (ESI†). Note that the enthalpies of formation without the zero point energy (ZPE) correction are only ~0.07 eV per atom different from the ZPE-corrected energies, and convex hulls are not sensitive to ZPE. Thus, for reasons of computational convenience, the zero point energy is omitted for the systematic structural search.

3.1 Rocksalt TiN and related subnitrides $Ti_{n+1}N_n$

While TiN has the ideal cubic rocksalt structure, Ti_3N_2, Ti_4N_3 and Ti_6N_5 are versions of this structure with ordered N-vacancies (see Fig. 2) – in Ti_3N_2 one third of nitrogen sites are vacant, in Ti_4N_3 – one quarter, and in Ti_6N_5 – one sixth. Similar vacancy-ordered phases were reported earlier to be stable for hafnium and titanium carbides $M_{n+1}C_n$ (M = Hf and n = 2, 5;[45] M = Ti and n = 1, 2, 5 [46]). Generally, the decrease of vacancy concentration makes the structure denser, less compressible, harder, and more stable under pressure. Indeed, among defective rocksalt phases only Ti_6N_5 (with the lowest vacancy concentration) survives as a (barely) stable phase at 60 GPa. Ti_3N_2 has space group *Immm*, while Ti_4N_3 and Ti_6N_5 belong to space group *C*2/*m*. It is convenient to visualize these structures by N-centered octahedral (NTi_6), as shown in Fig. 2. In the $Ti_{n+1}N_n$ series, Ti_5N_4 is missing as a stable compound. Nevertheless, a structure with space group *I*4/*m* is very close to the convex hull, but lies above it (15 meV per atom), *i.e.*, Ti_5N_4 is a metastable phase. The convex hull diagram of the Ti–N system at finite temperatures is shown in Fig. S1 (ESI†). The results yield a conclusion that none of the Ti–N compounds will lose their thermodynamic stability up to 1000 K.

ε-Ti_2N has the anti-rutile structure with space group $P4_2/mnm$. At pressures above 20.8 GPa (Fig. S3, ESI†), tetragonal ε-Ti_2N transforms into an orthorhombic *Cmcm* structure (see Fig. 2d). This structure contains a distorted close packing of Ti atoms, where one half of octahedral voids are occupied by nitrogen atoms, and edge-sharing NTi_6-octahedra form double slabs alternating with nitrogen-free layers. It is noteworthy that the enthalpy of *Cmcm*-Ti_2N is lower by more than 0.24 eV f.u.$^{-1}$ than that of the Au_2Te-type or Al_2Cu-type structures proposed by Ivashchenko *et al.*[23]

Having investigated the crystal structures and energetics of the various titanium subnitrides $Ti_{n+1}N_n$ and TiN, we now consider their electronic properties. The total and partial densities of states (DOS) of the ground-state compounds are shown in Fig. 3. The crystal orbital Hamilton population (–COHP) curves were calculated by using the LOBSTER package[47] and are displayed in Fig. 4. These orbital-pair interactions can provide a quantitative measure of bond strengths. The positive and negative energy regions in the –COHP curves correspond to bonding and antibonding states, respectively. For $Ti_{n+1}N_n$ structures, the DOS are decomposed

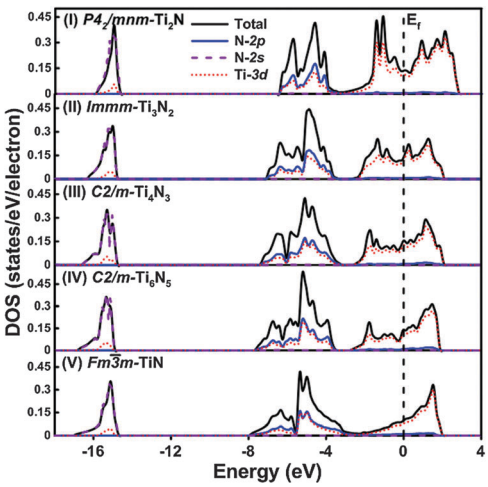

Fig. 3 The total and partial density of states (DOS) for the $Ti_{n+1}N_n$ subnitrides and TiN at zero pressure. The vertical dashed line is the Fermi energy.

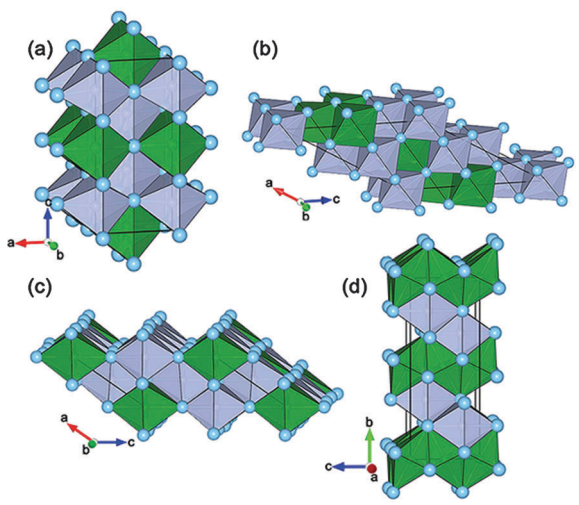

Fig. 2 Crystal structures of Ti–N compounds. (a) *Immm*-Ti_3N_2 at 0 GPa, (b) *C*2/*m*-Ti_4N_3 at 0 GPa, (c) *C*2/*m*-Ti_6N_5 at 0 GPa, and (d) *Cmcm*-Ti_2N at 60 GPa. The Ti and N atoms are represented as big blue and small gray spheres, respectively; nitrogen vacancies are shown as the green octahedra.

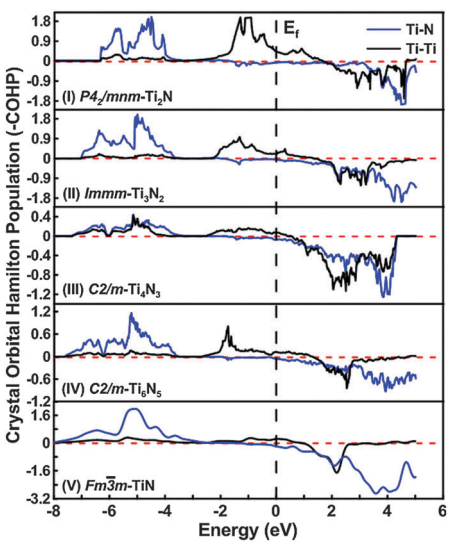

Fig. 4 The calculated crystal orbital Hamilton population (–COHP) for the $Ti_{n+1}N_n$ subnitrides and TiN at zero pressure.

into three well separated energy regions: (1) a deeply lowest valence band, s_N; (2) a hybridized Ti-3d/N-2p band, d_Mp_N; (3) a partially filled higher lying Ti-3d band, d_M. The s_N band is dominated by the 2s orbitals of the nitrogen atoms. Therefore, the contribution of this band to the bonding is not so large. The following upper group of valence bands d_Mp_N is a result of strong hybridization from the 3d states of Ti atoms and the 2p states of N atoms. These peaks correspond to the Ti-3d/N-2p bonding orbital contribution. Their antibonding counterparts appear well above the Fermi level.

When n goes from 1 to 5 in $Ti_{n+1}N_n$ series, *e.g.*, the number of N-filled Ti_6 octahedra increases, the energy region for the Ti-3d/N-2p peaks is expanded. This energy dispersion is caused by more extensive mixing between Ti-3d and N-2p orbitals, and suggests the enhancement of the covalency of the titanium–nitrogen bonding network. Let us turn our discussion to the upper energy region. From both DOS and COHP analyses, one may see that the bottom of the d_M band is mainly dominated by the bonding orbitals of 3d Ti atoms and the corresponding DOS exhibits a feature of the ''near free electron'' responsible for metallicity (see Fig. 3). Vacant antibonding Ti-3d/N-2p and antibonding Ti-3d/N-3d states compose the bottom of the conduction band. These results confirm the mixed covalent Ti–N and metallic Ti–Ti bonding nature in titanium subnitrides and TiN compounds.

As N content increases, valence band broadens (d_Mp_N band), valence electron concentration increases, and covalent interactions become stronger. This is reflected in shortening of Ti–N bonds: the shortest bond lengths are 2.082, 2.071, 2.069 and 2.022 Å for Ti_2N, Ti_3N_2, Ti_4N_3 and Ti_6N_5 at 0 GPa, respectively. In the same sequence the $N(E_F)$ gradually decreases, reaching the lowest value of ~0.098 states per eV per electron for TiN (see Fig. 3). To further explore the bonding nature in each $Ti_{n+1}N_n$ and TiN structures, we examined the electron localization function (ELF)[48] of these Ti–N compounds (see Fig. 5). We find that there are relatively large ELF values between Ti and N atoms, indicating the partially covalent Ti–N interactions. ELF = 0.5 can be identified between titanium atoms, suggesting metallic Ti–Ti bonding. All of these results are consistent with the discussion about the DOS and COHP for each structure of Ti_xN_y. Also, we can find charge transfer from Ti to N atoms, consistent with Holec *et al.*[49]

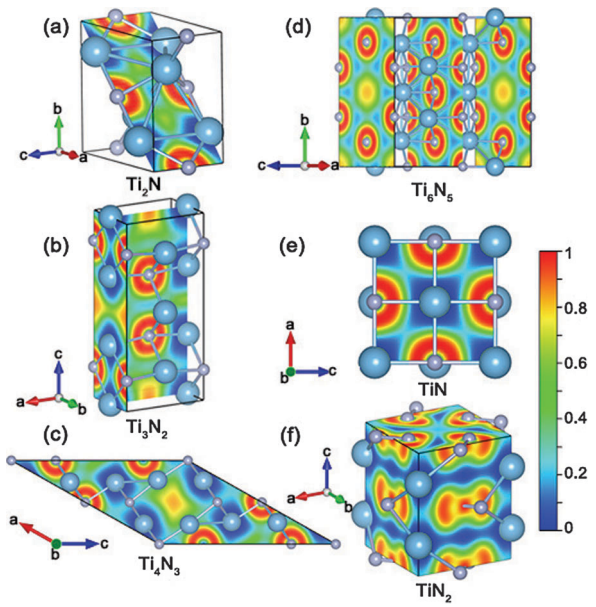

Fig. 5 Calculated electron localization function (ELF) maps for the Ti–N compounds. The blue spheres represent Ti atoms while gray spheres represent N atoms.

3.2 TiN_2, a high-pressure structure with N_2 dumbbells

At 60 GPa, we uncovered a nitrogen-rich compound TiN_2 with the $CuAl_2$-type structure (SG: *I*4/*mcm*, see Fig. 6a). The formation enthalpy of this *I*4/*mcm* structure is lower than that of the previously proposed thermodynamic ground state, the CaC_2-V-type structure, predicted by Kulkarni *et al.*[50] at 60 GPa. This new structure is stable against the decomposition into the mixture of TiN and N_2 at pressures above 26.6 GPa (Fig. S4, ESI†). To examine the stability of the *I*4/*mcm* structure, the phonon frequencies were calculated at atmospheric pressure and at 60 GPa, which are shown in Fig. 6b and Fig. S2 (ESI†). Imaginary phonon frequencies were not observed in the entire Brillouin zone, indicating that the predicted *I*4/*mcm* structure is dynamically stable and, if synthesized, might be quenchable at atmospheric pressure.

The structure of TiN_2 contains TiN_8 face-sharing tetragonal antiprisms stacked along the *c*-axis. Unlike normal $CuAl_2$-type structures, here we have N_2-dumbbells encapsulated in cubic Ti_8 hexahedra. This topology is identical to the recently predicted stable high-pressure magnesium oxide MgO_2.[51] The N–N bond length is calculated to be 1.348 Å and 1.378 Å at 60 GPa and 1 atm, respectively. Projected N-2p DOS shows that antibonding $1\pi_g^*$ levels are almost fully occupied at 60 GPa (see Fig. 6c).

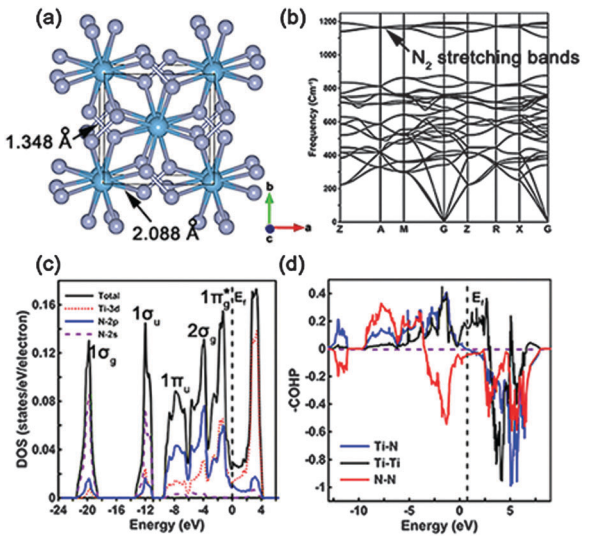

Fig. 6 (a) Crystal structure of *I*4/*mcm*-TiN_2, (b) the phonon dispersion curve at 60 GPa, (c) projected and total DOS with symmetry labels of molecular N_2^{4-} filled valence orbitals assigned to each DOS peak at 60 GPa, and (d) –COHP of *I*4/*mcm*-TiN_2 at 60 GPa.

Consequently, for electron counting purposes, the dinitrogen units should be formally considered as N_2^{4-}, a pernitride unit isoelectronic to fluorine F_2 molecules. Its electronic ground state configuration is $1\sigma_g^2 1\sigma_u^2 1\pi_u^4 2\sigma_g^2 1\pi_g^{*4}$ for 14 valence electrons and its bond order is one (Fig. S5, ESI†). Formally, this leaves the titanium atoms of TiN_2 in a d^0 configuration (Ti^{4+}). Note that a large variety of structures are known with the square antiprismatic geometry and a formally d^0 metal center such as TaF_8^{3-} in Na_3TaF_8.[52]

Stabilizing Ti–Ti interactions in binary Ti–N structures is weakening when nitrogen content increases, *e.g.*, when formal valence d electrons d^n decrease (Ti oxidation number increases). This behavior is structurally reflected by the elongation of the Ti–Ti distances with increasing nitrogen content (shortest Ti–Ti bonds of 2.255 Å and 2.517 Å in Ti_2N and TiN_2 at 60 GPa, respectively). Note that the pernitride N_2^{4-} units point directly towards the tetragonal faces of the eight-coordinated titanium atoms (Ti–N bonding length is 2.088 Å at 60 GPa) and are perpendicular to each other in order to minimize the steric clashes between the nitrogen σ-lone pairs (Pauli repulsions).

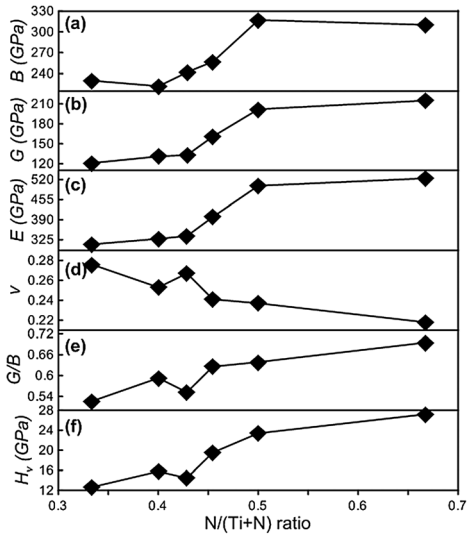

Fig. 7 Calculated bulk modulus *B*, shear modulus *G*, Young's modulus *E*, Poisson's ratio *ν*, *G*/*B* ratio, and Vickers hardness H_v of the titanium nitrides as a function of N content.

3.3 Mechanical properties of Ti–N stable structures

The mechanical stability was examined by using the calculated elastic constants (see Table 1), and we found that all these phases satisfy the Born–Huang stability criteria.[53] Our calculated elastic constants are in good agreement with the available data.[6,54–56] One can note the large C_{33} values for Ti_2N, Ti_4N_3, TiN and especially TiN_2 (653 GPa from the GGA and 729 GPa from the LDA), which indicate very low compressibility along the *c*-axis. For TiN_2, we also find a very large elastic constant C_{44} (336 GPa from the GGA and 364 GPa from the LDA).

The calculated bulk modulus *B* and shear modulus *G* are also listed in Table 1 and the trend of these mechanical properties as a function of N content for the ground-state structures is shown in Fig. 7. Our calculated results for the well-known rock-salt TiN and ε-Ti_2N are in good agreement with reported values,[6,54–56] supporting the accuracy and reliability for other Ti–N compounds. Among these titanium nitrides, TiN has the largest *B* of 294 GPa from the GGA and 339 GPa from the LDA, which can be comparable to WB_4 with a bulk modulus of 328 GPa.[57] A minimum of *B* appears in Ti_3N_2, because this is a vacancy-rich rock-salt phase, and due to the large concentration of vacancies it has unexpectedly low C_{12} and C_{22} values as listed in Table 1.

The shear modulus measures the resistance to the shape change at constant volume and provides a much better correlation with hardness than bulk modulus.[60] TiN_2 has the largest shear modulus of 197 GPa from the GGA and 233 GPa from the LDA, which suggests that TiN_2 is the hardest material among the titanium nitrides. Fig. 8 shows the directional dependence of Young's moduli for the considered Ti–N compounds, and one can clearly see anisotropy from the deviations of its shape from sphere. The Young's modulus along the *c*-axis direction is higher than that along the other directions for Ti_2N, Ti_4N_3 and TiN_2, which agrees well with our above analysis on elastic constants. The Young's modulus is more isotropic in Ti_4N_3 and Ti_6N_5, while Ti_2N, Ti_3N_2 and TiN_2 show more anisotropy

Table 1 The calculated elastic constants C_{ij}, bulk modulus *B* (GPa), shear modulus *G* (GPa), Young's modulus *E* (GPa), Poisson's ratio *ν*, *κ* = *G*/*B* ratio, and Vickers hardness H_v (GPa) of the Ti–N compounds at 0 GPa

Phase		C_{11}	C_{12}	C_{13}	C_{16}	C_{22}	C_{23}	C_{26}	C_{33}	C_{36}	C_{44}	C_{45}	C_{55}	C_{66}	*B*	*G*	*E*	*ν*	*κ*	H_v
Ti_2N	GGA	300	214	115					442		157			137	214	112	287	0.277	0.523	11.87
($P4_2/mnm$)	LDA	353	235	138					489		184			147	246	130	332	0.275	0.528	13.38
Ti_3N_2	GGA	458	99	125		400	115		332		119		145	86	206	124	309	0.250	0.602	15.53
($Immm$)	LDA	545	113	140		449	140		370		127		172	92	237	138	347	0.256	0.583	16.00
Ti_4N_3	GGA	368	150	155	−17	393	119	3	421	−29	140	10	126	114	225	125	317	0.265	0.556	14.05
($C2/m$)	LDA	412	181	179	−16	444	135	8	484	−42	167	19	139	130	258	141	357	0.269	0.547	14.84
Ti_6N_5	GGA	424	140	145	−20	429	146	20	429	1	147	21	158	171	238	151	373	0.239	0.634	18.97
($C2/m$)	LDA	484	161	175	−33	490	175	33	481	1	166	34	187	201	275	170	424	0.243	0.618	20.07
TiN	GGA	590	145								169				294	189	466	0.235	0.643	22.55
($Fm\bar{3}m$)	LDA	704	157								183				339	215	533	0.238	0.634	24.22
	GGA[6]	583	129								179				278					24.19[58]
	LDA[6]	698	139								198				321					
	Exp[54]	625	165								163				320					23.00[59]
TiN_2	GGA	535	279	71					653		336			148	284	197	481	0.218	0.693	25.64
($I4/mcm$)	LDA	631	301	106					729		364			185	335	233	567	0.218	0.696	28.75

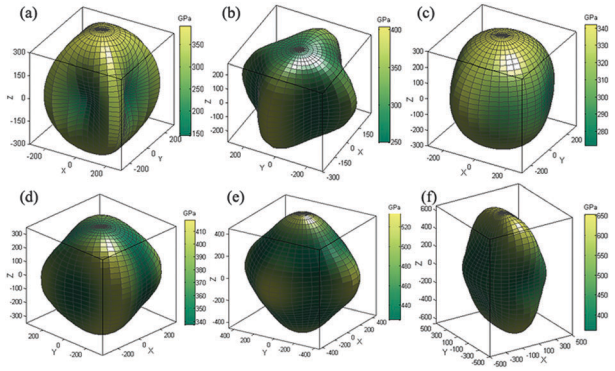

Fig. 8 Directional dependence of Young's moduli (in GPa) for (a) $P4_2/mnm$-Ti_2N, (b) $Immm$-Ti_3N_2, (c) $C2/m$-Ti_4N_3, (d) $C2/m$-Ti_6N_5, (e) $Fm\bar{3}m$-TiN and (f) $I4/mcm$-TiN_2.

than other Ti–N compounds. For Ti_2N, the anisotropy is mainly because of its high C_{12} and low C_{11}. Ti_3N_2 has just the opposite situation, the low C_{12} and high C_{11} make Young's modulus large in the axis direction and small in the diagonal direction. For TiN_2, it is mainly because of its high C_{44} (Table 1).

Poisson's ratio ν and the G/B ratio[61] are indicative of the degree of directionality of covalent bonding. A typical value of ν is $\sim$0.2 for strong directional covalent materials and $\sim$0.4 for metals. A low Poisson's ratio results from directional bonds, which increase the shear modulus and limit the motion of dislocations, thereby increasing the material's hardness. From Fig. 7, we find that ν drops down from Ti_2N to TiN_2 with increasing N content, except Ti_4N_3, which shows a local maximum. For Ti_4N_3, we can find that there is significant Ti–Ti metallic bonding in contrast with other Ti–N compounds (see Fig. 4). The large Ti–Ti metallic bonds impair the covalency of this phase, which leads to a local minimum of hardness (see Fig. 7f).

The Vickers hardness was estimated by Chen's empirical method for the ground-state vacancy-ordered Ti–N compounds and is listed in Table 1. Among the Ti–N compounds, TiN_2 has the largest hardness of 26 GPa from the GGA and 29 GPa from the LDA. Note that this is an orientationally averaged value (anisotropy is not considered in eqn (1)). It is no wonder that increasing nitrogen content changes bonding to more directional, the more N is added, the more Ti–N bonds are formed and the less Ti–Ti bonding remains. Based on the analysis of the electronic properties and chemical bonding in those stable Ti–N compounds, we can conclude that with increasing N content, the enhancement of directional covalent interactions and decline of metallicity lead to the increase of the hardness.

4 Conclusions

In summary, we have extensively explored the stable structures and possible stoichiometries in the Ti–N system at 0, 20 and 60 GPa by first-principles evolutionary crystal structure prediction. In addition to the well-known phases Ti_2N and TiN, we have uncovered three new intriguing structures under ambient conditions (Ti_3N_2, Ti_4N_3 and Ti_6N_5). At high pressures, two new phases $Cmcm$-Ti_2N and $I4/mcm$-TiN_2 were discovered. All those phases are mechanically and dynamically stable under ambient conditions. The calculated elastic constants C_{ij} are in good agreement with the available reported data. Other mechanical properties including the bulk modulus, the shear modulus, Young's modulus, and Poisson's ratio have been further computed from C_{ij}. Among the studied Ti–N compounds, TiN_2 possesses the highest hardness of 26 GPa from the GGA and 29 GPa from the LDA. We found a strong correlation between the mechanical properties and N content for the ground-state structures, *i.e.*, the more N content, the more directional covalent Ti–N bonding and the less Ti–Ti metallic bonding, which lead to the enhancement of the hardness. The materials discovered here are attractive for technological applications because of a compromise between hardness and ductility, due to a peculiar interplay between metallicity and covalency.

Acknowledgements

We thank the Natural Science Foundation of China (Grants no. 51372203 and 51332004), the Basic Research Foundation of NWPU (Grant no. JCY20130114), the Foreign Talents Introduction and Academic Exchange Program (Grant no. B08040), the National Science Foundation (Grants no. EAR-1114313 and no. DMR-1231586), DARPA (Grants no. W31P4Q1310005 and W31P4Q1210008), and the Government of the Russian Federation (Grant no. 14.A12.31.0003) for financial support. The authors also acknowledge the High Performance Computing Center of NWPU for the allocation of the computing time on their machines.

References

1 H. O. Pierson, *Handbook of refractory carbides and nitrides: properties, characteristics, processing, and applications*, Noyes Publications, 1996.
2 R. Buhl, H. Pulker and E. Moll, *Thin Solid Films*, 1981, **80**, 265–270.
3 M. Wittmer, B. Studer and H. Melchior, *J. Appl. Phys.*, 1981, **52**, 5722–5726.
4 E. Valkonen, T. Karlsson, B. Karlsson, *et al.*, 1983 International Techincal Conference/Europe, 1983, pp. 375–381.
5 M. Stoehr, C.-S. Shin, I. Petrov and J. Greene, *J. Appl. Phys.*, 2011, **110**, 083503.
6 K. Liu, X. Zhou, H. Chen and L. Lu, *Phys. B*, 2012, **407**, 3617–3621.
7 M. Brik and C. Ma, *Comput. Mater. Sci.*, 2012, **51**, 380–388.
8 Y. Yang, H. Lu, C. Yu and J. Chen, *J. Alloys Compd.*, 2009, **485**, 542–547.
9 L. H. Dubois, *Polyhedron*, 1994, **13**, 1329–1336.
10 L. H. Dubois, B. R. Zegarski and G. S. Girolami, *J. Electrochem. Soc.*, 1992, **139**, 3603–3609.
11 A. Sherman, *J. Electrochem. Soc.*, 1990, **137**, 1892–1897.
12 P. Blaha and K. Schwarz, *Int. J. Quantum Chem.*, 1983, **23**, 1535–1552.

13 P. Blaha, J. Redinger and K. Schwarz, *Phys. Rev. B: Condens. Matter Mater. Phys.*, 1985, **31**, 2316.
14 T. Marten, E. I. Isaev, B. Alling, L. Hultman and I. A. Abrikosov, *Phys. Rev. B: Condens. Matter Mater. Phys.*, 2010, **81**, 212102.
15 P. Mayrhofer, F. Kunc, J. Musil and C. Mitterer, *Thin Solid Films*, 2002, **415**, 151–159.
16 K. Weinert and M. Schneider, *Influence of the grinding process on the process behaviour of cutting tools*, Springer, 1999.
17 F. Bannister, *Mineral. Mag.*, 1941, **26**, 36–44.
18 J. Zhao, L. Yang and Y. Yu, *et al.*, *Chin. Phys. Lett.*, 2005, **22**, 1199.
19 P. Ojha, M. Aynyas and S. P. Sanyal, *J. Phys. Chem. Solids*, 2007, **68**, 148–152.
20 R. Chauhan, S. Singh and R. K. Singh, *Cent. Eur. J. Phys.*, 2008, **6**, 277–282.
21 B. Holmberg, *Acta Chem. Scand.*, 1962, **16**, 13.
22 C. De Novion and J. Landesman, *et al.*, *Pure Appl. Chem.*, 1985, **57**, 1391–1402.
23 V. Ivashchenko, P. Turchi, V. Shevchenko and E. Olifan, *Phys. Rev. B: Condens. Matter Mater. Phys.*, 2012, **86**, 064109.
24 P. Kroll, *J. Phys.: Condens. Matter*, 2004, **16**, S1235.
25 A. R. Oganov and C. W. Glass, *J. Chem. Phys.*, 2006, **124**, 244704.
26 A. R. Oganov, Y. Ma and A. O. Lyakhov, *et al.*, *Rev. Mineral. Geochem.*, 2010, **71**, 271–298.
27 A. R. Oganov, A. O. Lyakhov and M. Valle, *Acc. Chem. Res.*, 2011, **44**, 227–237.
28 A. R. Oganov, Y. Ma, A. O. Lyakhov, M. Valle and C. Gatti, *Rev. Mineral. Geochem.*, 2010, **71**, 271–298.
29 G. Kresse and J. Furthmüller, *Phys. Rev. B: Condens. Matter Mater. Phys.*, 1996, **54**, 11169.
30 A. R. Oganov, *Modern methods of crystal structure prediction*, John Wiley & Sons, 2011.
31 P. Hohenberg and W. Kohn, *Phys. Rev.*, 1964, **136**, B864.
32 W. Kohn and L. J. Sham, *Phys. Rev.*, 1965, **140**, A1133.
33 J. P. Perdew, K. Burke and M. Ernzerhof, *Phys. Rev. Lett.*, 1996, **77**, 3865.
34 P. E. Blöchl, *Phys. Rev. B: Condens. Matter Mater. Phys.*, 1994, **50**, 17953.
35 D. Ceperley, B. Alder, S. H. Vosko, L. Wilk and M. Nusair, *Can. J. Phys.*, 1980, **58**, 1200.
36 H. J. Monkhorst and J. D. Pack, *Phys. Rev. B: Condens. Matter Mater. Phys.*, 1976, **13**, 5188–5192.
37 A. Togo, F. Oba and I. Tanaka, *Phys. Rev. B: Condens. Matter Mater. Phys.*, 2008, **78**, 134106.
38 R. Hill, *Proc. Phys. Soc., London, Sect. A*, 1952, **65**, 349.
39 W. Voigt, *Lehrbuch derKristallphysik*, Teubner, Leipzig, 1928.
40 A. Reuss and Z. Angnew, *Math. Methods*, 1929, **9**, 55.
41 X. Chen, H. Niu, D. Li and Y. Li, *Intermetallics*, 2011, **19**, 1275–1281.
42 G. Ghosh, A. van de Walle and M. Asta, *Acta Mater.*, 2008, **56**, 3202–3221.
43 Y. K. Vohra and P. T. Spencer, *Phys. Rev. Lett.*, 2001, **86**, 3068.
44 R. Bini, L. Ulivi, J. Kreutz and H. J. Jodl, *J. Chem. Phys.*, 2000, **112**, 8522–8529.
45 Q. Zeng, J. Peng, A. R. Oganov and Q. Zhu, *et al.*, *Phys. Rev. B: Condens. Matter Mater. Phys.*, 2013, **88**, 214107.
46 C. Jiang and W. Jiang, *Phys. Status Solidi B*, 2014, **251**, 533–536.
47 R. Dronskowski and P. E. Bloechl, *J. Phys. Chem.*, 1993, **97**, 8617–8624.
48 A. D. Becke and K. E. Edgecombe, *J. Chem. Phys.*, 1990, **92**, 5397–5403.
49 D. Holec, R. Rachbauer and D. Kiener, *et al.*, *Phys. Rev. B: Condens. Matter Mater. Phys.*, 2011, **83**, 165122.
50 A. Kulkarni, J. Schön, K. Doll and M. Jansen, *Chem. – Asian J.*, 2013, **8**, 743–754.
51 Q. Zhu, A. R. Oganov and A. O. Lyakhov, *Phys. Chem. Chem. Phys.*, 2013, **15**, 7696–7700.
52 J. K. Burdett, R. Hoffmann and R. C. Fay, *Inorg. Chem.*, 1978, **17**, 2553–2568.
53 Z. Wu, E. Zhao and H. Xiang, *et al.*, *Phys. Rev. B: Condens. Matter Mater. Phys.*, 2007, **76**, 054115.
54 R. Ahuja, O. Eriksson, J. M. Wills and B. Johansson, *Phys. Rev. B: Condens. Matter Mater. Phys.*, 1996, **53**, 3072–3079.
55 J. Kim, J. Achenbach and P. Mirkarimi, *et al.*, *J. Appl. Phys.*, 1992, **72**, 1805–1811.
56 A. Wang, S. Shang and Y. Du, *et al.*, *Comput. Mater. Sci.*, 2010, **48**, 705–709.
57 M. Wang, Y. Li and T. Cui, *et al.*, *Appl. Phys. Lett.*, 2008, **93**, 101905.
58 Z. Jiao, S. Ma, X. Zhang and X. Huang, *Europhys. Lett.*, 2013, **101**, 46002.
59 A. Szymanski and J. M. Szymanski, *Hardness estimation of minerals, rocks and ceramic materials*, Elsevier Press, Amsterdam, 1989.
60 H.-Y. Chung, M. B. Weinberger, J.-M. Yang, S. H. Tolbert and R. B. Kaner, *Appl. Phys. Lett.*, 2008, **92**, 261904.
61 S. Pugh, *Philos. Mag.*, 1954, **45**, 823–843.